


RESEARCH

Open Access



Enhancing differentiation and functionality of insulin-producing cells derived from iPSCs using esterified collagen hydrogel for cell therapy in diabetes mellitus

Ji Eun Moon^{1†}, Yu Na Lee^{1†}, Sehui Jeong^{1,2}, Hye Ryeong Jun¹, Minh Hien Hoang^{1,2}, Yeonggwon Jo³, Jinah Jang^{3,4}, In Kyong Shim^{1,2,5*}  and Song Cheol Kim^{1,2,6*}

Abstract

Background Islet transplantation is a recommended treatment for type 1 diabetes but is limited by donor organ shortage. This study introduces an innovative approach for improving the differentiation and functionality of insulin-producing cells (IPCs) from iPSCs using 3D spheroid formation and hydrogel matrix as an alternative pancreatic islet source. The extracellular matrix (ECM) is crucial for pancreatic islet functionality, but finding the ideal matrix for β -cell differentiation has been challenging. We aimed to advance IPC differentiation and maturation through an esterified collagen hydrogel, comparing its effectiveness with conventional basement membrane extract (BME) hydrogels.

Methods iPSCs were differentiated into IPCs using a small molecule-based sequential protocol, followed by spheroid formation in concave microwells. Rheological analysis, scanning electron microscopy, and proteomic profiling were used to characterize the chemical and physical properties of each matrix. IPCs, both in single-cell form and as spheroids, were embedded in either ionized collagen or BME hydrogels, which was followed by assessments of morphological changes, pancreatic islet-related gene expression, insulin secretion, and pathway activation using comprehensive analytical techniques.

Results Esterified collagen hydrogels markedly improved the structural integrity, insulin expression, and cell-cell interactions in IPC spheroids, forming densely packed insulin-expressing clusters, in contrast to the dispersed cells observed in BME cultures. Collagen hydrogel significantly enhanced the mRNA expression of crucial endocrine markers and maturation factors, with IPC spheroids showing accelerated differentiation from day 5, suggesting a faster differentiation compared to single cells in hydrogel encapsulation. Insulin secretion in response to glucose in collagen environments, with a GSIS index of 2.46 ± 0.05 , exceeded those in 2D and BME, demonstrating superior

[†]Ji Eun Moon and Yu Na Lee authors contributed equally to this work.

*Correspondence:
In Kyong Shim
shimiink@gmail.com
Song Cheol Kim
drksc@amc.seoul.kr

Full list of author information is available at the end of the article



© The Author(s) 2024. **Open Access** This article is licensed under a Creative Commons Attribution-NonCommercial-NoDerivatives 4.0 International License, which permits any non-commercial use, sharing, distribution and reproduction in any medium or format, as long as you give appropriate credit to the original author(s) and the source, provide a link to the Creative Commons licence, and indicate if you modified the licensed material. You do not have permission under this licence to share adapted material derived from this article or parts of it. The images or other third party material in this article are included in the article's Creative Commons licence, unless indicated otherwise in a credit line to the material. If material is not included in the article's Creative Commons licence and your intended use is not permitted by statutory regulation or exceeds the permitted use, you will need to obtain permission directly from the copyright holder. To view a copy of this licence, visit <http://creativecommons.org/licenses/by-nc-nd/4.0/>.

pancreatic islet functionality. Pathway analysis highlighted enhanced insulin secretion capabilities, evidenced by the upregulation of genes like Secretogranin III and Chromogranin A in collagen cultures. In vivo transplantation results showed that collagen hydrogel enhanced cluster integrity, tissue integration, and insulin secretion compared to non-embedded IPCs and BME groups.

Conclusion Esterified collagen hydrogels demonstrated superior efficacy over 2D and BME in promoting IPC differentiation and maturation, possibly through upregulation of the expression of key secretion pathway genes. Our findings suggest that using collagen hydrogels presents a promising approach to enhance insulin secretion efficiency in differentiating pancreatic β -cells, advancing cell therapy in diabetes cell therapy.

Keywords Diabetes, Induced pluripotent stem cells, Differentiation, Insulin-producing cells, Extracellular matrix (ECM), Collagen

Background

Diabetes mellitus (DM) presents a global health challenge characterized by persistently high blood sugar levels that impose significant burdens on individuals and healthcare systems worldwide. Type 1 DM stems from an autoimmune assault on pancreatic islets, resulting in the failure of insulin production by β -cells [1]. Despite remarkable progress in therapeutic interventions, managing Type 1 DM remains challenging, typically necessitating intensive insulin regimens and continuous glucose monitoring to avert complications and achieve optimal glycemic control [2]. Pancreatic islet transplantation has emerged as a promising strategy, offering the potential to not only alleviate symptoms but essentially restore the pancreas' original function, thereby improving the quality of life of affected individuals [3, 4]. However, the limited availability of pancreatic islets poses a considerable challenge to the widespread application of this treatment, catalyzing the exploration of alternative approaches such as stem cell-derived insulin-producing cell (IPC) therapy [5–8].

Advancements in stem cell differentiation technologies have paved the way toward generating IPCs. Nevertheless, these cells often fall short of fully mimicking the mature physiological functions characteristic of human pancreatic islet cells. Pancreatic islets, also known as the islets of Langerhans, comprise clusters of endocrine α , β , and δ cells intricately nestled within the pancreas. The architectural organization of these islets, optimizing cell–cell interactions, particularly among β -cells, is crucial for the development of a mature insulin secretion pattern [9–11]. The 3D structure of islets facilitates complex interactions and communication between cells, playing essential roles in the regulation of blood glucose levels and metabolism in response to glucose intake [12, 13].

The extracellular matrix (ECM), crucial for maintaining the 3D structure of pancreatic islets, significantly enhances their functionality and survival [11]. Current 3D culture techniques often utilize basement membrane extract (BME), such as Matrigel, which comprises various components like laminin, collagen type IV, and growth factors. However, the derivation of BME from mouse

tumor tissues and its composition predominantly of tumor-derived proteins limit its direct clinical applicability. Given these constraints and the need for ECM alternatives that better mimic the specific properties required by different cells and tissues, collagen—a primary ECM component renowned for its structural and tensile strength—has emerged as a viable candidate [14–17].

Collagen, widely used in clinical settings such as surgery and orthopedics, has proven safety. Its biocompatibility, derived from being a biological component, enhances the function of transplanted cells and offers exceptional physical properties. Notably, our previous research demonstrated that esterified collagen can hydrate in neutral pH and its degradation rate can be controlled, making it highly clinically useful [18, 19]. Its cationic surface properties also improve cell attachment and functionality. Furthermore, several reports have enhanced the functionality of other biopolymers like hyaluronic acid through esterification [20, 21]. This study aims to assess the effectiveness of esterified collagen hydrogel as a supportive matrix for iPSC-derived IPCs. By comparing the differentiation and maturation capabilities of IPCs embedded in collagen hydrogel versus those in BME, our research endeavors to advance pancreatic islet cell therapy for diabetes treatment, highlighting a promising direction with regard to overcoming current limitations in stem cell-derived therapies.

Methods

Induced pluripotent stem cells (iPSC) culture and differentiation into IPCs

Induced pluripotent stem cells (iPSCs) were provided by the Center for Stem Cell Research, Asan Medical Center, Seoul, Korea. The study involving induced pluripotent stem cells (iPSCs) was approved by the Institutional Review Board (IRB) of Asan Medical Center, Seoul, Korea (Project Title: Preferential lineage-specific differentiation of iPSC derived from human pancreas-derived cells into insulin-producing cells; Approval Number: 2917–0503; Approval Date: 2017-04-28).

The iPSCs were maintained on dishes coated with vitronectin (Gibco, Carlsbad, CA, USA) and cultured in StemMACS iPS-Brew XF Human medium (Miltenyi Biotec, Bergisch Gladbach, Germany) supplemented with 10 μM Y-27,632 (Selleck, Houston, TX, USA) at 37 °C in a 5% CO₂ atmosphere.

Induced pluripotent stem cells (iPSC) culture and differentiation into IPCs

For in vitro differentiation into insulin-producing cells (IPCs), a sequential differentiation protocol utilizing small molecules was employed. This protocol guided the iPSCs through stages of definitive endoderm, pancreatic progenitor cell specification, and IPC maturation [22]. The differentiation process, including the media and factors used at each stage, is illustrated in Fig. 1A.

For in vivo transplantation, a more refined protocol was used to enhance the differentiation efficiency of iPSCs into IPCs. This refined protocol included five stages, following a previously reported method [23]. Each stage medium was prepared with specific factors in MCD131 medium (Gibco) as follows: definitive endoderm stage with 10 ng/ml activin A and 3 μM CHIR99021, primitive gut tube stage with 50 ng/ml KGF, pancreatic progenitor stage 1 with 50 ng/ml KGF, 0.2 μM TPPB, 0.25 μM Sant1, 2 μM retinoic acid, and 0.2 μM LDN, pancreatic progenitor stage 2 with 50 ng/ml KGF, 0.2 μM TPPB, 0.25 μM Sant1, 0.1 μM RA, and 0.2 μM LDN, and endocrine progenitor stage with 10 μM heparin, 1 μM XXi, 10 μM Alk5i II, 1 μM T3, 0.25 μM Sant1, 0.1 μM RA, and 10 μM forskolin.

Spheroid formation of IPCs

IPC spheroids were generated using StemFIT 3D concave microwells (Microfit, Gyeonggi-do, Korea) pre-coated with 3% (w/v) bovine serum albumin (BSA; Cellnest, NJ, USA) to prevent cell adhesion. Pancreatic progenitor cells were seeded into these microwells, forming spheroids approximately 150 μm in diameter within 24 h.

Hydrogel embedding

The formed IPC spheroids were encapsulated in either ionized collagen hydrogel (CollaShield[®]; Dalim Tissen, Korea) or BME hydrogel (Cultrex[®] Basement Membrane Extract, Type 2; R&D Systems, MN, USA). Esterified collagen (EC) was produced by dissolving 1% (w/v) EC (Dalim Tissen, Seoul, Korea) in 0.1 M acetic acid (Junsei Chemical, Tokyo, Japan). The freeze-dried EC underwent crosslinking with 20 mM of 1-ethyl-3-(3-dimethylamino-propyl) carbodiimide hydrochloride (EDC; Tokyo Chemical, Tokyo, Japan) within an ethanol solution (Merck Millipore, MA, USA). This embedding process involved mixing cell suspensions (IPCs) and IPC spheroids with the respective hydrogel formulations and transferring

them into culture wells to form a dome shape, followed by gelation at 37 °C for 30 min.

Hydrogel characterization

The physical and chemical properties of the hydrogels were evaluated using various characterization techniques. Rheological properties were assessed using the Advanced Rheometric Expansion System (TA Instruments, DE, USA). Collagen hydrogels at different concentrations were investigated using a Discovery Hybrid Rheometer-2 (TA Instruments, USA) with a steel 20 mm parallel plate geometry. A steady shear sweep test was conducted at 4 °C to determine the shear viscosities of the collagen hydrogels in the pre-gel state. Oscillatory frequency sweep tests analyzed the storage (G') and loss (G'') moduli under a 2% strain and a frequency range of 0.1–100 rad s⁻¹, after incubating the pre-gels at 37 °C for 30 min. An oscillatory temperature sweep test evaluated the gelation kinetics of the collagen hydrogels from 4 °C to 37 °C at a heating rate of 5 °C min⁻¹. For comparison, commercially available 1% BME hydrogel was used as a control. The same rheological tests, including steady shear sweep, oscillatory frequency sweep, and oscillatory temperature sweep, were performed on the BME hydrogel under the same conditions. All tests were performed in triplicate.

Scanning electron microscopy (SEM) (AIS1800C; Saron, Gyeonggi-do, Korea) visualized the surface morphology of freeze-dried hydrogel samples.

The ECM compositions of collagen and BME hydrogels were identified using high-resolution liquid chromatography-mass spectrometry-based proteomic analysis. Samples underwent in-solution protein digestion to form peptides. The procedure began with 8 M urea in 0.1 M ammonium bicarbonate to achieve a final concentration of at least 6 M. For reduction and alkylation, a mixture of 10 mM dithiothreitol and 30 mM iodoacetamide was applied. Following this step, 10 μg of Trypsin/Lys-C protease mix was added, and the samples were incubated at 37 °C for 16 h. To stop the digestion, 0.4% trifluoroacetic acid was added, and the samples were desalted using C18 Harvard macro spin columns. The resulting peptides were lyophilized, reconstituted in 100 μL of 0.1% formic acid, and quantified using a Q Exactive Plus Hybrid Quadrupole-Orbitrap mass spectrometer coupled with a Nanoacquity UPLC (Waters, Manchester, UK). Elution was performed through a trap column, and ionization was facilitated by an NSI system linked with a fused-silica column packed with 2 μm C18 particles, operating at an electric potential of 2.0 kV. During the MS/MS process, the maximal ion injection time and dynamic exclusion time were set to 60 ms and 30 s, respectively. Proteomic analysis was conducted using a Dionex UltiMate 3000 RSLCnano system (Thermo Fisher Scientific) coupled

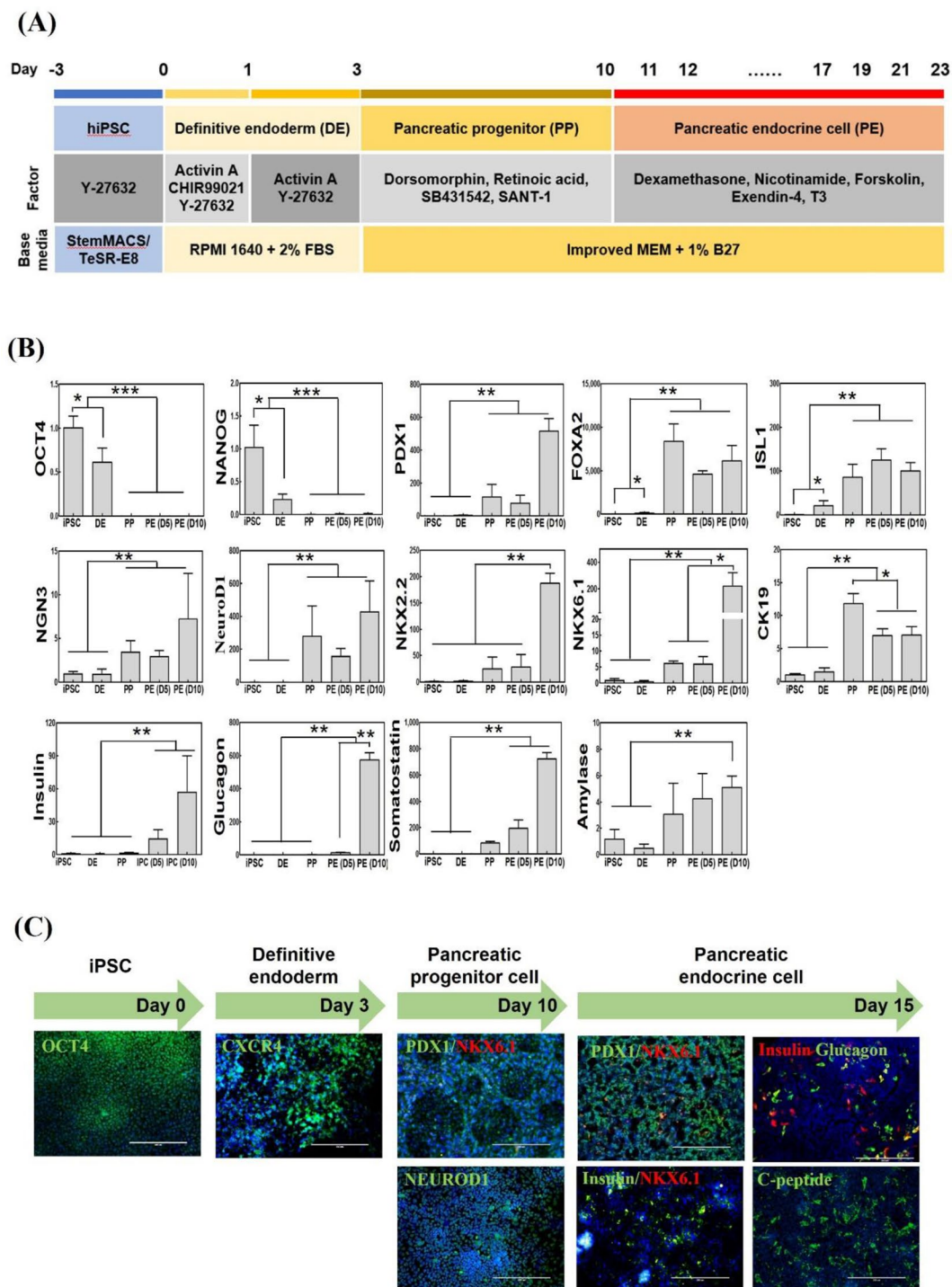


Fig. 1 Differentiation of iPSCs into Pancreatic Endocrine Cells **(A)** A schematic of the differentiation protocol outlining the media composition and factors used at each stage to generate pancreatic endocrine cells (PE) from human induced pluripotent stem cells (hiPSCs). **(B)** Representative mRNA expression levels of genes associated with pancreatic lineage, endocrine hormones, and iPSC-specific markers at different stages: iPSC, definitive endoderm (DE), pancreatic progenitor (PP), early pancreatic endocrine (early PE), and late pancreatic endocrine (late PE) stages ($n=3$). Significance levels are denoted by $*p<0.05$, $**p<0.005$, and $***p<0.001$, with experiments performed in triplicate ($n=3$). **(C)** Immunocytochemistry images demonstrate the differentiation milestones: OCT4 (green) expression in iPSCs; CXCR4 (green) expression in definitive endoderm; PDX1 (green)/NKX6.1 (red) and NEUROD1 (green) expression in pancreatic progenitors; and PDX1 (green)/NKX6.1 (red), insulin (red)/glucagon (green), insulin (green)/NKX6.1 (red), and C-peptide (green) expression in late pancreatic endocrine cells. Nuclei are stained with DAPI (blue). Scale bars: 200 μ m. Magnification: 20x

with a Q Exactive Plus mass spectrometer (Thermo Fisher Scientific). Proteome Discoverer software (Version 2.2; Thermo Fisher Scientific) processed the data, with protein identification and characterization performed by searching against the reviewed Human Uniprot-SwissProt protein database. The mass spectrometry data supporting the results reported in this paper are available as Supplementary Material.

Quantitative real-time PCR (qPCR)

Following RNA extraction using TRIzol reagents (Thermo Fisher Scientific) and cDNA synthesis (SuperScript III First-Strand Synthesis System, Thermo Fisher Scientific), qRT-PCR was conducted on the LightCycler® 480 II system (Roche Applied Science) using SYBR Green I Master mix (Roche Applied Science). Primer sets are listed in Table 1. The PCR amplification program included an initial polymerase activation step at 95 °C

for 5 min, followed by 40 cycles of denaturation at 95 °C for 10 s, annealing at 57 °C for 20 s, and extension/detection at 72 °C for 40 s. Gene expression was normalized to GAPDH, with the delta CT method used to quantify relative expression levels. Statistical analyses were conducted using one-way analysis of variance (ANOVA) followed by a *post hoc* Tukey's test.

Flow cytometry

3D cell clusters were dissociated into single cells using TrypLE™ (Thermo Fisher Scientific) and washed with phosphate-buffered saline (PBS). Cells were stained with BD Horizon™ Fixable Viability Stain 450 (BD Biosciences) to assess viability. For intracellular staining, cells were fixed and permeabilized using the BD Cytofix/Cytoperm™ Fixation/Permeabilization Kit (BD Biosciences). Nuclear permeabilization and staining were performed using the True-Nuclear™ Transcription Factor Buffer Set (BioLegend). Primary antibodies against C-peptide (rat anti-C-peptide, DSHB, GN-ID4-S, 1:300 dilution) and NKX6.1 (mouse anti-NKX6.1, DSHB, F55A12-S, 1:100 dilution) were used. Secondary antibodies conjugated to fluorophores were applied, followed by nuclear staining with DAPI. Flow cytometry analysis was performed using a Canto™ II flow cytometer (BD Biosciences), and data were analyzed using FlowJo software.

Viability assessment

Cell viability was assessed using trypan blue exclusion. Briefly, IPC spheroids were dissociated into single cells using TrypLE™, diluted in media, and mixed with an equal volume of 0.4% trypan blue (Gibco). Cell viability was determined using a LUNA-II™ Automated Cell Counter (Logos Biosystems).

Immunofluorescence staining

Cells on slides were permeabilized with 0.1% Triton X-100 and blocked with 3% BSA for 1 h. Primary antibodies used included mouse anti-OCT4 (1:100; Santa Cruz Biotechnology, sc-5279), goat anti-CXCR4 (1:300; Abcam, ab1670), mouse anti-NEUROD1 (1:200; Abcam, ab60704), mouse anti-glucagon (1:200; Abcam, ab10988), rabbit anti-insulin (1:200; Abcam, ab181547), goat anti-PDX1 (1:200; R&D Systems, AF2419), rat anti-C-peptide (DSHB, GN-ID4-S), and mouse anti-NKX6.1 (DSHB, F55A12-S). Samples were incubated with primary antibodies overnight at 4 °C. For secondary antibody labeling, cells were incubated with anti-rabbit IgG Cy3 (1:200; Bethyl Laboratories, A120-201C3), anti-goat IgG Alexa Fluor 488 (1:300; Thermo Fisher Scientific, A11055), anti-mouse IgG Alexa Fluor 488 (1:300; Thermo Fisher Scientific, A11029), anti-mouse IgG Alexa Fluor 555 (1:300; Thermo Fisher Scientific, A21203), and anti-rat IgG Alexa Fluor 488 (1:300; Thermo Fisher Scientific,

Table 1 Primer list for qPCR

Genes		5'–3'
OCT4	Forward	GTGGAGGAAGCTGACAACAA
	Reverse	AACAAATTCTCCAGGTGCC
NANOG	Forward	CTGGCTGAATCCTTCCTCTC
	Reverse	CATGAGATTGACTGGATGGG
PDX1	Forward	GCATCCCAGGTCTGTCTTCT
	Reverse	CACTGCCAGAAAGGTTTGAA
FOXA2	Forward	TCCGACTGGAGCAGCTACTATG
	Reverse	CCACGTACGACGACATGTTC
ISL1	Forward	ATTTCCCTATGTGTTGGTTGGC
	Reverse	CGTTCTTGCTGAAGCCGATG
NGN3	Forward	CTGGCTGAATCCTTCCTCTC
	Reverse	CATGAGATTGACTGGATGGG
NKX2.2	Forward	CGGCGAGTGCTTTTCTCCAA
	Reverse	GCGTTCATCTTGTAGCGG
NKX6.1	Forward	CACACGAGACCCACTTTTTTC
	Reverse	CCGCCAAGTATTTTGTTCCT
CK19	Forward	AACGGCGAGCTAGAGGTGA
	Reverse	GGATGGTCGTGTAGTAGTGCC
Insulin	Forward	GCAGCCTTTGTGAACCAACAC
	Reverse	CCCCGCACACTAGGTAGAGA
Glucagon	Forward	CCCAAGATTTTGTGCAGTGGTT
	Reverse	GCGGCCAAGTCTTCAACAAT
Somatostatin	Forward	CTGTCTGAACCCCAACCCAGAC
	Reverse	CAGCTCAAGCCTCATTTTCAT
Amylase	Forward	TTCAGACCTTGGTGGGAAAGA
	Reverse	ACGAACCCCAACATTGTACAT
Secretogranin III	Forward	GTCTTCATCAACTAGACGGGACT
	Reverse	ACAATCTTGTCAAACCGGCTC
Chromogranin	Forward	TAAAGGGGATACCGAGGTGATG
	Reverse	TCGGAGTGCTCAAACATTCC
Secretagogin	Forward	AACTGGGTACTGATGACACGG
	Reverse	TCTTTAGAGGCATCTTGGGTAGT
GAPDH	Forward	GAAGGTGAAGTCCGGAGT
	Reverse	GAAGATGGTGATGGGATTC

A21208) for 2 h at 25 °C. Nuclei were stained using DAPI (Invitrogen, D1306).

TUNEL staining was performed using the in-situ cell death detection kit (Roche Diagnostics GmbH, Mannheim, Germany) following the manufacturer's protocol. Samples were imaged using the EVOS® FL Auto Cell Imaging System (Thermo Fisher Scientific).

Enzyme-linked immunosorbent assay (ELISA)

Insulin and C-peptide levels were quantified using ELISA kits (Alpco, NH, USA; Mercodia, Uppsala, Sweden) according to the manufacturers' protocols. Glucose-stimulated insulin secretion assays involved incubating cells in Krebs-Ringer bicarbonate (KRB) buffer with varied glucose concentrations, determining the stimulation index based on insulin secretion ratios under high- versus low-glucose conditions. For the glucose-stimulated insulin secretion assay, IPCs and IPC spheroids were incubated in KRB buffer (128 mM NaCl, 5 mM NaHCO₃, 1 mM NaHCO₃, 5mM KCl, 2.7 mM CaCl₂, 1.2 mM KH₂PO₄, 1.2 mM MgCl₂, and 10 mM HEPES, 0.5% BSA) with varying glucose concentrations at 37 °C. The buffer contained glucose concentrations of 2 mM, 20 mM, and 20 mM with 30 mM KCl. Following sequential incubations, supernatants were collected, and the stimulation index was calculated as the ratio of insulin secretion in high-glucose media to that secreted in low-glucose media.

Microarray analysis of the IPC spheroids in collagen or BME hydrogel

Gene expression in IPC spheroids embedded in different hydrogels was profiled using Agilent SurePrint G3 Human GE 8×60 K V3 Microarrays (Agilent Technologies), following the manufacturer's protocols. Raw data were extracted using the Agilent Feature Extraction Software (v11.0.1.1), and array probes with Flag A in samples were filtered out. The selected processed signal value was log-transformed and normalized using the quantile method. The statistical significance of the expression data was determined using fold changes of more than 2 between two groups. Data analysis, including normalization, was performed with R software, complemented by protein-protein interaction analysis via the STRING database. The microarray data supporting the results reported in this paper are available as Supplementary Material.

In vivo Assessment of IPC spheroids and esterified collagen hydrogel

The animal experiments were conducted with the approval of the Institutional Animal Care and Use Committee (IACUC) at the Asan Institute for Life Sciences (Project Title: Experiments on differentiation and

diabetes control of insulin-producing cells produced by 3D culture; Approval Number: 2022-12-212; Approval Date: 2022-08-16). All procedures adhered to relevant guidelines and regulations. This study was conducted in accordance with the ARRIVE guidelines 2.0 to ensure the rigorous and reproducible reporting of animal research. A completed ARRIVE checklist has been submitted along with this manuscript. The anesthesia method used was isoflurane, and euthanasia was performed by CO₂ inhalation. IPC spheroids ($n=3$ groups: non-embedded, BME hydrogel-embedded, and collagen hydrogel-embedded) were prepared and subcutaneously implanted into the dorsal region of 8-week-old male diabetic nude mice (10⁷ cells per transplant). Blood serum from non-transplanted diabetic mice served as a negative control. Human C-peptide levels were measured using a human C-peptide ELISA kit to assess insulin secretion. After four weeks, mice were euthanized, and tissues were harvested, fixed in 10% formalin, embedded in paraffin, sectioned (4 μm), and stained with hematoxylin and eosin (H&E). Immunohistochemistry was performed using rat anti-C-peptide primary antibodies.

The in vivo degradation rate of esterified collagen hydrogel was evaluated in 8-week-old SD rats. One milliliter of collagen hydrogel was subcutaneously injected into the dorsal region of rats ($n=4$). Animals were euthanized at specific time points (days 1, 3, 7, 14, 21, 28, 42, 56, and 70), and implants were recovered, lyophilized, and weighed to determine degradation rate.

Statistical analysis

We performed all statistical analyses using GraphPad Prism 8.0.1 (GraphPad Software, San Diego, CA, USA). We evaluated between-group differences using one-way analysis of variance and post-hoc analysis after a normality test. We corrected errors with Tukey's method in the post-hoc analysis. We considered data with $p<0.05$ as statistically significant.

Results

iPSC differentiation into IPCs

Under the conditions of our experiment, we validated a differentiation protocol for induced pluripotent stem cells (iPSCs). Quantitative mRNA analysis conducted at the end of each differentiation stage revealed a significant reduction in the expression of the pluripotency markers OCT4 and NANOG following definitive endoderm (DE) induction. Concurrently, we observed an increase in the expression of transcription factors essential for initiating pancreatic lineage differentiation, namely PDX1, FOXA2, ISL1, NKX2.2, and NKX6.1, as depicted in Fig. 1B. From the pancreatic progenitor (PP) stage, there was a notable increase in the expression of specific genes such as PDX1, FOXA2, ISL1, NGN3, NKX2.2, and NKX6.1, confirming

the onset of pancreatic lineage commitment. Notably, at the pancreatic endocrine (PE) stage on day 10 (D10), there was a marked increase in the levels of PDX1, NGN3, NeuroD1, NKX2.2, and NKX6.1, which are critical markers for IPC differentiation.

This enhancement in expression suggests a successful progression toward IPC phenotypes. The morphological evidence for their differentiation into pancreatic progenitor cells was provided through immunostaining with established markers, as shown in Fig. 1C. Collectively, these results indicate the successful differentiation of iPSCs into a pancreatic progenitor phenotype, setting the stage for their potential maturation into functional pancreatic islet-like cells in our optimized experimental setup.

Rheological characterization and structural analysis of hydrogels

We evaluated the gelation and rheological properties of various collagen concentrations and 1% BME hydrogels. Collagen at 0.5% concentration did not gel after a 60-minute incubation period. In contrast, 1% and 1.5% collagen concentrations exhibited successful gelation. Rheological measurements showed that 1% collagen hydrogel closely matched the modulus of 1% BME gel at a low shear rate (Fig. 2A). Cross-linked hydrogels of both collagen and BME remained stable over a broad range of shear frequencies (0.1–1000 rad/s). SEM imaging provided insight into the microstructure of the hydrogels, revealing that both 1% and 1.5% collagen and 1% BME hydrogels possessed a highly porous architecture suitable for cellular transport and biomolecule diffusion (Fig. 2B). The main protein components of the hydrogels were quantified; collagen hydrogels were predominantly composed of

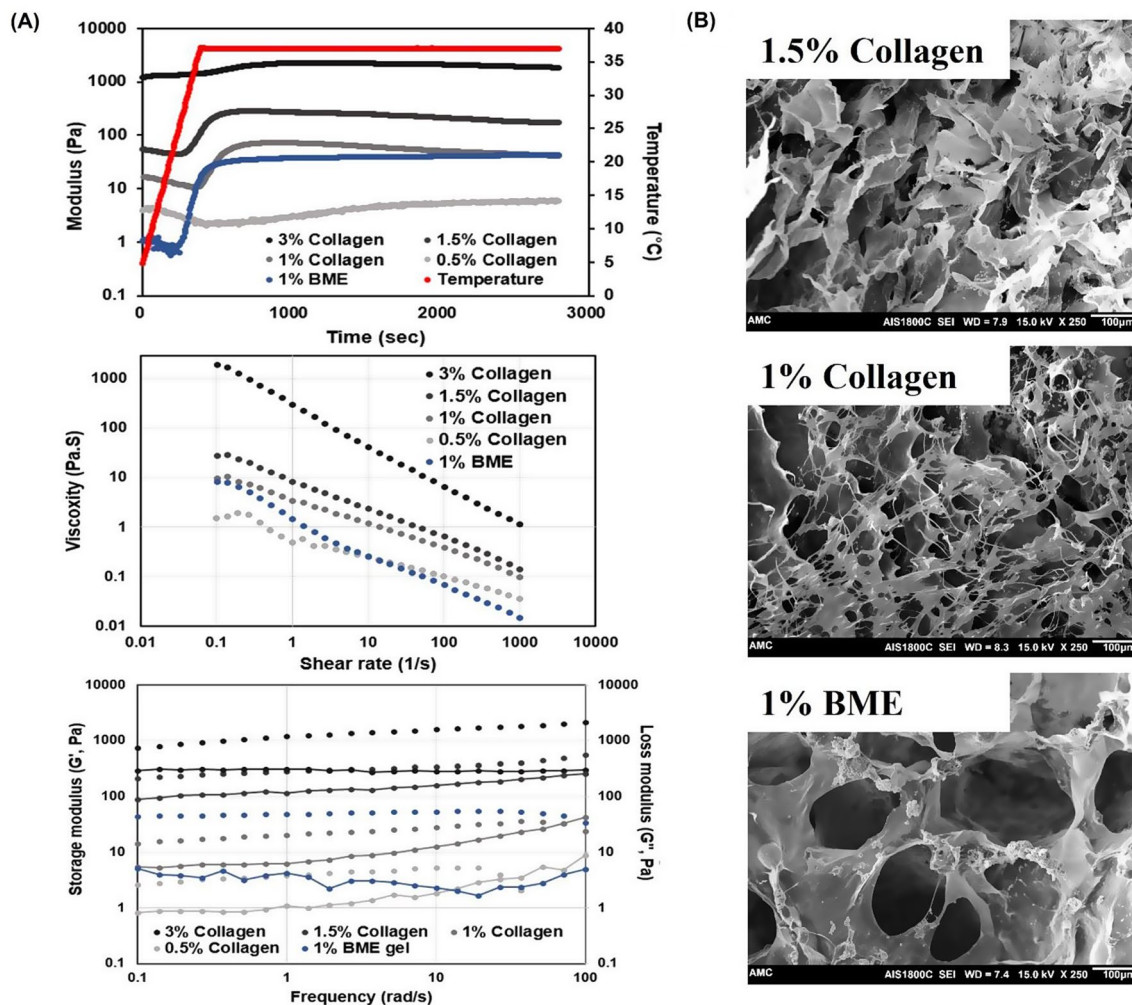


Fig. 2 Rheological and Structural Properties of BME and Collagen Hydrogels (A) Rheological behavior of BME and collagen hydrogels, illustrating gelation kinetics and stability. The modulus over time and response to shear rate and frequency were analyzed for 1% BME and collagen hydrogels at varying concentrations (0.5%, 1%, 1.5%, and 3%). (B) Scanning electron microscopy (SEM) images showcasing the porous structure of 1% BME, 1% collagen, and 1.5% collagen hydrogels

collagen type I alpha 1 chain (65.77%), while BME hydrogels were rich in laminin subunits (alpha-1, beta-1, and gamma-1), comprising 77.5% of the total protein content (Table 2).

Morphological changes in IPCs and IPC spheroids in collagen and BME hydrogels

Our experimental setup involved the cultivation of IPC spheroids using microconcave wells and subsequently embedding these spheroids, as well as IPC suspensions, into collagen and BME hydrogels. Figure 3A shows the microscopy images of iPCs and IPC spheroid both in microconcave wells and suspensions. Observations on days 1 and 10 revealed that IPCs and IPC spheroids in the BME hydrogel, where single cells and spheroids frequently transitioned into cyst-like structures, reminiscent of ducts (Fig. 3B, indicated by red arrows). IPC spheroids retained their shape better in collagen than in BME hydrogels over 10 days. Collagen-embedded spheroids showed denser packing, indicative of more robust cell–cell interactions. Following a 10-day culture period, immunolabeling for insulin was performed. In BME hydrogels, insulin-positive cells were sparsely distributed, whereas collagen hydrogels showed abundant insulin-positive cell clusters, indicative of advanced differentiation (Fig. 3C).

To compare collagen-embedded spheroids with non-embedded spheroids and evaluate the impact of collagen embedding on the generation of insulin-producing cells (IPCs), we performed immunocytochemistry (ICC) and flow cytometry analyses. These analyses compared the expression of C-peptide and the maturation marker NKX6.1 between the groups. In both the non-embedded and collagen-embedded groups, cells formed intact

spheroidal morphologies and displayed differentiated C-peptide-positive cells (Fig. 3D). IPC spheroids cultured in both BME and collagen hydrogels exhibited a higher number of C-peptide-expressing cells than non-embedded IPCs, with a notable increase in NKX6.1 expression specifically in the collagen-embedded group.

Cell viability assays using trypan blue staining demonstrated no significant differences in cell survival between the groups (viability rates: non-embedded: $87.5 \pm 2.6\%$, BME: $88.33 \pm 1.6\%$, collagen: $87.17 \pm 5.6\%$). Similarly, TUNEL staining indicated no apoptosis in the hydrogel-embedded cells, suggesting that both collagen and BME hydrogels are biocompatible.

Gene expression in IPCs and IPC spheroids within collagen and BME hydrogels

After a 10-day culture period, IPCs in collagen hydrogels demonstrated substantial increases in the expression of islet hormone genes compared to pancreatic progenitor cells prior to embedding. The expression of INS increased by 46.75 ± 3.13 -fold in 2D cultures, 210.65 ± 37.03 -fold in BME, and 278.14 ± 47.14 -fold in collagen. GCG levels escalated to 137.29 ± 59.18 in 2D, 189.43 ± 18.22 in BME, and reached 584.73 ± 93.99 in collagen. Similarly, SST levels rose to 8.66 ± 2.03 in 2D, 8.62 ± 2.86 in BME, and significantly increased to 63.69 ± 10.60 in collagen (Fig. 4A). Although the increase in gene expression for IPC spheroids in collagen was consistent, significant enhancement was noted as early as day 5, signifying accelerated differentiation relative to single cells in hydrogels (Fig. 4B). CK19 levels, which signify non-endocrine or duct-like differentiation, remained consistently low across all conditions without significant variance (0.35 ± 0.11 for 2D, 0.29 ± 0.04 for BME, and 0.38 ± 0.07 for Collagen),

Table 2 Composition of Collagen and BME Hydrogel Proteins

Collagen			BME		
Gene Name	Protein Name	Percent (%)	Gene Name	Protein Name	Percent (%)
COL1A1	Collagen type I alpha 1 chain	65.77	Lama1	Laminin subunit alpha-1	37.16
KRT5	Keratin 5	13.29	Lamb1	Laminin subunit beta-1	23.69
COL3A1	Collagen alpha-1(III) chain precursor	11.44	Nid1	Nidogen-1	17.36
FAM98A	Family with sequence similarity 98 member A	4.59	Lamc1	Laminin subunit gamma-1	16.61
DSPP	DSPP600	3.37	Hspg2	Basement membrane-specific heparan sulfate proteoglycan core protein	1.67
ALB	Serum albumin	0.55	Pxdn	Peroxidasin homolog	0.42
KRT84	Keratin 84	0.31	Fn1	Fibronectin	0.19
COL1A2	Collagen alpha-2(I) chain precursor	0.27	Hist1h4a	Histone H4	0.18
FLG2	Filaggrin family member 2	0.13	Serpinh1	Serpin H1	0.17
PSCA	Prostate stem cell antigen	0.07	Myh4	Myosin-4	0.14
ANXA2	Annexin	0.06	Nid2	Nidogen-2	0.12
KRT10	Keratin 10	0.06	Actb	Actin, cytoplasmic 1	0.12
HIST1H2B	Histone H2B	0.05	Fgg	Fibrinogen gamma chain	0.12

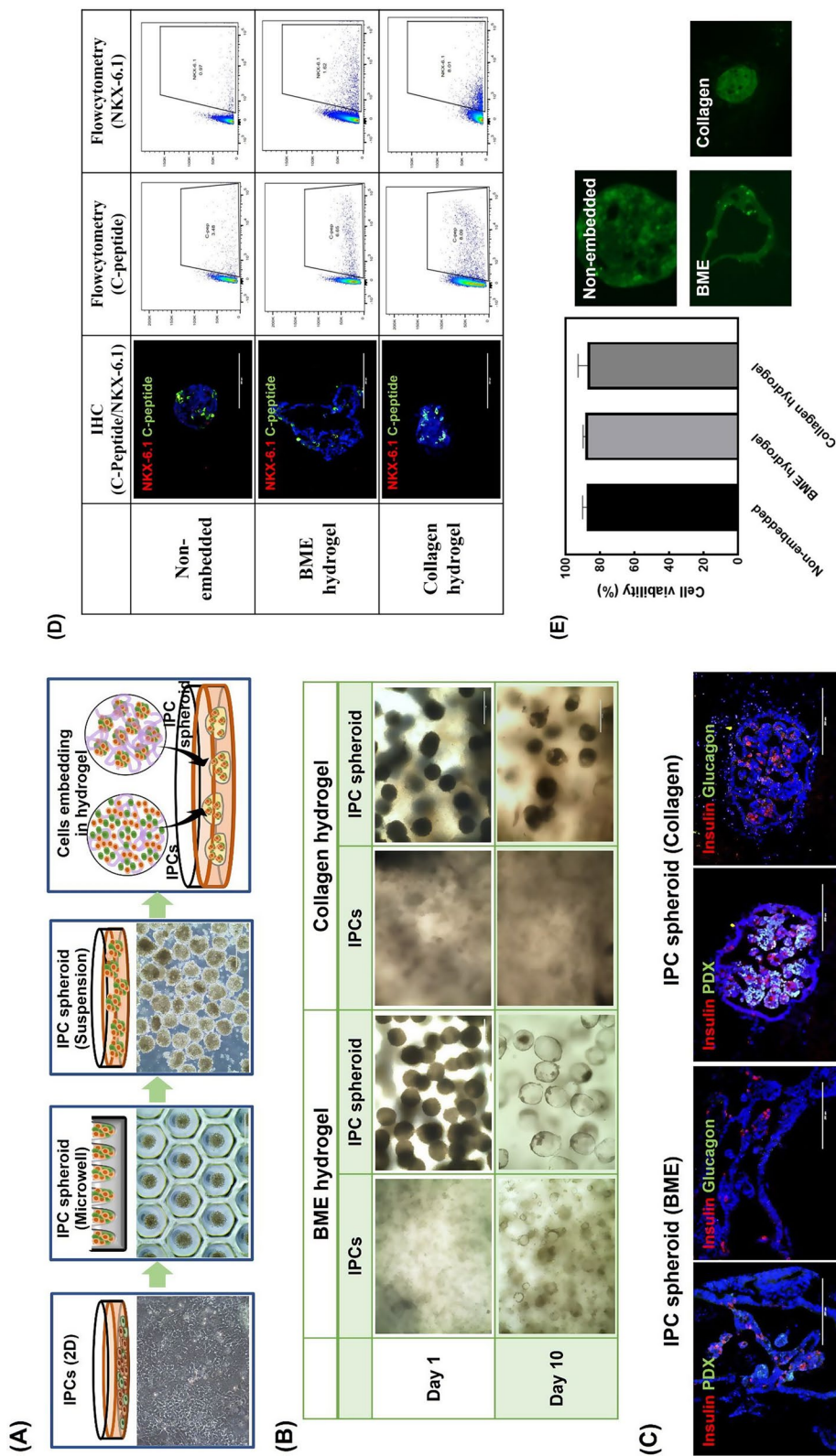
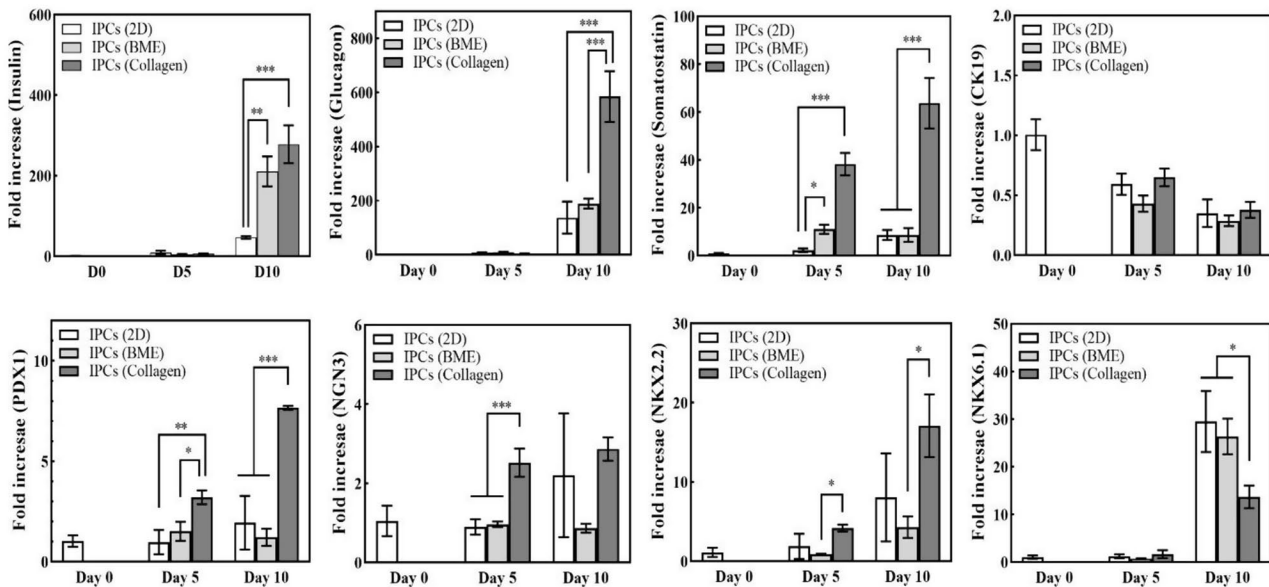


Fig. 3 Differentiation and Morphological Integrity of IPCs in Collagen and BME Hydrogels **(A)** Schematic representation of IPC spheroid generation and embedding in hydrogels, illustrating the transition from 2D culture to 3D spheroid culture in microconcave wells and suspension culture, followed by embedding in hydrogel matrices. **(B)** Microscopic observation of IPCs and IPC spheroids embedded in collagen and BME hydrogels, captured on days 1 and 10. BME hydrogels show cyst-like structures, while collagen hydrogels maintain spheroidal integrity. Scale bars: 400 μ m, 10x magnification. **(C)** Immunocytochemical analysis of IPC spheroids demonstrating insulin (red), PDX1 (green), and glucagon (green) expression. Collagen hydrogels exhibit dense insulin-positive clusters, indicative of advanced differentiation. Scale bars: 200 μ m, 20x magnification. **(D)** IHC and flow cytometry analysis comparing non-embedded, BME, and collagen hydrogel-embedded IPC spheroids. IHC images display C-peptide (green) and NKX6.1 (red) expression. Flow cytometry plots quantify C-peptide and NKX6.1 expression levels. Scale bars: 200 μ m, 20x magnification. **(E)** Cell viability assessment using trypan blue staining (left panel). Representative TUNEL staining images demonstrating no apoptosis in hydrogel-embedded cells (right panel)

(A)



(B)

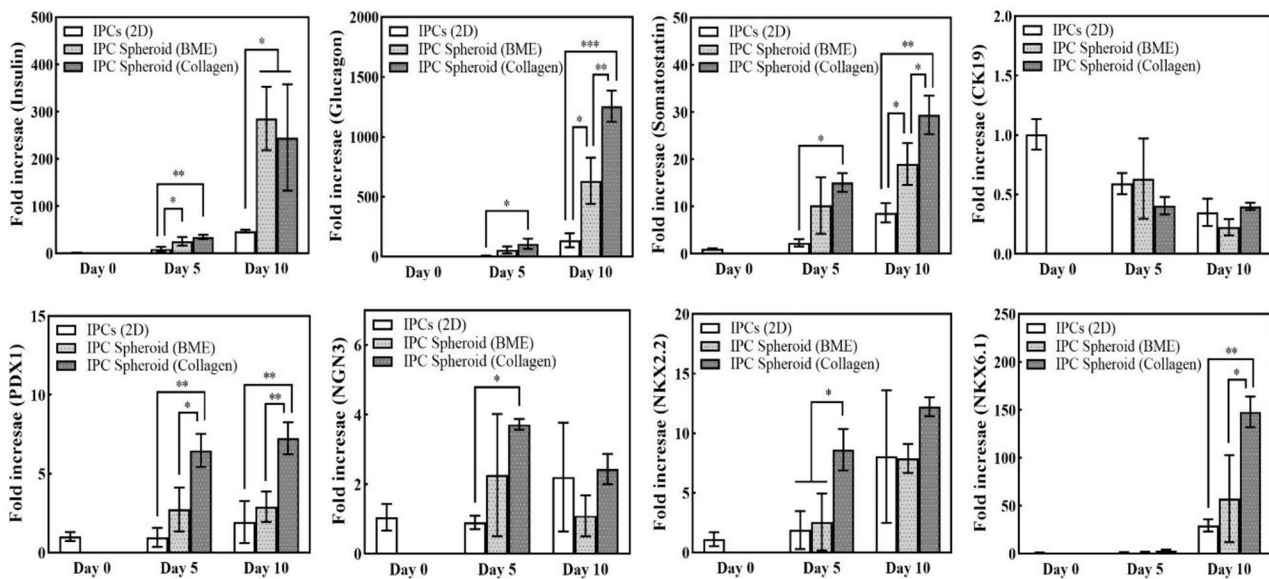


Fig. 4 mRNA Expression Profiles of IPCs and IPC Spheroids in Collagen and BME Hydrogels Relative mRNA expression levels of genes associated with pancreatic function and endocrine differentiation in (A) IPCs and (B) IPC spheroids. Pancreas-related and endocrine genes in (A) IPCs and (B) IPC spheroids cultured in collagen and BME hydrogels relative to a conventional 2D culture. These cells were cultured in either collagen or BME hydrogels, with results compared against traditional 2D culture systems. Post-encapsulation analyses were conducted at days 5 and 10. Significance levels are denoted by * $p < 0.05$, ** $p < 0.005$, and *** $p < 0.001$, with experiments performed in triplicate ($n = 3$)

indicating that while endocrine-related gene expression rose, undesirable differentiation was minimized and uniform. Furthermore, expression of PDX1, crucial for pancreatic functionality, notably increased in the collagen group, being 3.94 times higher than 2D and 6.81 times

higher than BME. While NKX6.1 expression showed no significant difference among single-cell groups, and a tendency to decrease in the collagen single-cell group compared to 2D, it surged in spheroids by day 10, with more than a fivefold increase in the collagen group compared

to 2D. In contrast, differentiation markers NGN3 and NKX2.2 showed increased expression in the collagen group by day 5, similar to trends observed in 2D cultures, but by day 10, the difference was not significant.

Insulin and C-peptide secretion profiles in IPCs and IPC spheroids

The functional maturation of IPCs was evaluated by measuring insulin and c-peptide secretion. Over time, both IPC suspensions and IPC spheroids embedded in hydrogels showed an increasing trend in insulin release, with a notable peak at day 13 (Fig. 5A). IPC spheroids, especially those in collagen hydrogels, exhibited the highest insulin and c-peptide levels. Measurement of c-peptide release on day 11 paralleled these findings, with collagen-embedded IPC spheroids demonstrating the most substantial secretion (Fig. 5B).

A glucose-stimulated insulin secretion (GSIS) assay revealed differential insulin secretion in response to glucose concentrations. Unlike 2D cultured cells, which showed negligible response, cells in hydrogels,

particularly those in collagen, responded to changes in glucose concentration. Collagen-embedded IPCs and IPC spheroids displayed the highest insulin secretion, indicating an enhanced glucose-responsive functionality similar to pancreatic islets (Fig. 5C and D).

Differential gene expression in Collagen enhances granule formation and insulin secretion

Microarray analysis was performed to explore the genetic basis for the observed insulin secretion functionality in IPC spheroids cultured in collagen versus BME hydrogels. To further understand the mechanisms underlying enhanced insulin secretion in IPC spheroids within collagen hydrogels, we identified a list of genes demonstrating more than a two-fold differential expression, as presented in Table 3. Interaction network analysis using STRING indicated a pronounced upregulation in the expression of transcription factors related to insulin-producing cells, growth factors, and cell–matrix interactions. Notably, the expression of genes involved in granule formation and secretion was particularly increased, suggesting

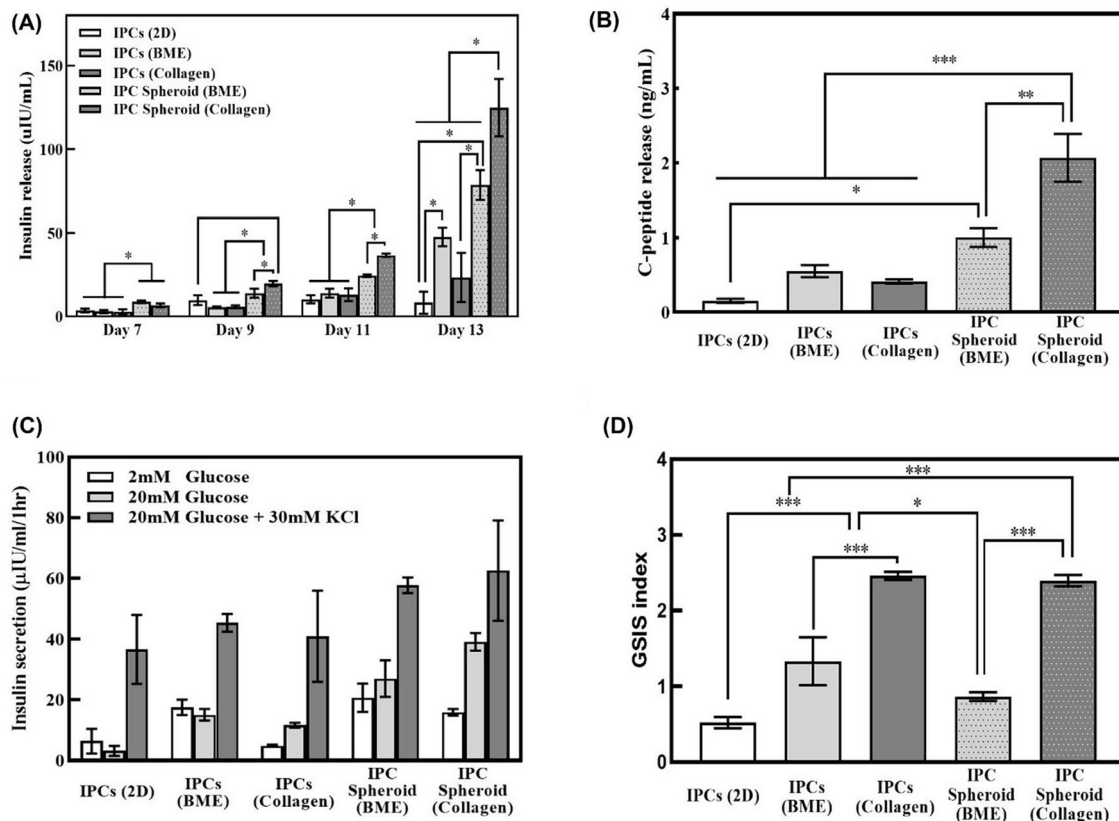


Fig. 5 Quantitative Analysis of Insulin and C-Peptide Production in IPC Hydrogel Cultures **(A)** Sequential insulin secretion in IPCs and spheroids within collagen and BME hydrogels, with day 13 showing peak levels for collagen. **(B)** C-peptide secretion levels measured on day 11. **(C)** Measurement of insulin secretion under varying glucose conditions, including low (2 mM) and high (20 mM) glucose, and high glucose with KCl (20 mM Glucose+30 mM KCl). **(D)** Glucose-stimulated insulin secretion (GSIS) index measuring insulin secretion response to glucose challenges. The GSIS index was calculated by comparing the amount of insulin secreted in high-glucose media to that in low-glucose media, confirming enhanced glucose responsiveness of IPCs in collagen hydrogels. (* $p < 0.05$, $n = 4$)

Table 3 Top upregulated genes in IPC spheroids in Collagen compared to BME hydrogels

Gene symbol	Genebank Accession	Description	Fold change
SCG3	NM_001165257	secretogranin III	5.09
RTL1	NM_001134888	retrotransposon-like 1	4.34
SPINK1	NM_003122	serine peptidase inhibitor, Kazal type 1	4.32
GCG	NM_002054	Glucagon	4.21
CPA2	NM_001869	carboxypeptidase A2 (pancreatic)	3.30
LYZ	NM_000239	Lysozyme	2.96
SOX2	NM_003106	SRY box 2	2.84
CRABP1	NM_004378	cellular retinoic acid binding protein 1	2.70
DLK1	NM_003836	delta-like 1 homolog (Drosophila)	2.53
LOC102723575	XR_913141	uncharacterized LOC102723575	2.51
CHGA	NM_001275	chromogranin A	2.36
OR52K2	NM_001005172	olfactory receptor, family 52, subfamily K, member 2	2.30
HS6ST3	NM_153456	heparan sulfate 6-O-sulfotransferase 3	2.29
STMN2	NM_001199214	stathmin 2	2.27
RFX4	NM_001206691	regulatory factor X, 4 (influences HLA class II expression)	2.25
CGA	NM_000735	glycoprotein hormones, alpha polypeptide	2.24
TM4SF4	NM_004617	transmembrane 4 L six family member 4	2.21
CDH10	NM_006727	cadherin 10, type 2 (T2-cadherin)	2.17
SST	NM_001048	Somatostatin	2.16
ADCY8	NM_001115	adenylate cyclase 8 (brain)	2.14
ZIC2	NM_007129	Zic family member 2	2.13
SCGN	NM_006998	secretagogin, EF-hand calcium binding protein	2.12
STXBPL	NM_001308330	syntaxin binding protein 5-like	2.10
ZIC5	NM_033132	Zic family member 5	2.09
ATP1A3	NM_001256213	ATPase, Na ⁺ /K ⁺ transporting, alpha 3 polypeptide	2.08
LOC102724094	NR_120519	uncharacterized LOC102724094	2.08

a potential role of these genes in enhancing glucose-responsive insulin secretion in collagen-embedded spheroids (Fig. 6A).

To verify the involvement of identified genes in insulin secretion, we conducted qPCR analysis to assess the mRNA expression levels of secretogranin III, chromogranin A, and secretagogin. In both IPCs and IPC spheroids cultured within collagen matrixes, all three genes exhibited increased expression, with the highest levels observed in IPC spheroids embedded in collagen, underscoring their contribution to the enhanced functionality of IPCs (Fig. 6B).

In vivo assessment of IPC spheroids and esterified collagen hydrogel

To evaluate the in vivo efficacy of esterified collagen hydrogel for IPC delivery, we subcutaneously implanted IPC spheroids in three groups: non-embedded, BME hydrogel-embedded, and collagen hydrogel-embedded, into diabetic nude mice. Histological analysis after four weeks revealed distinct outcomes (Fig. 7A). The BME group exhibited duct-like structures with scattered insulin-positive cells, while the collagen group maintained spheroid integrity, demonstrated improved tissue integration, and showed increased insulin expression. Non-embedded IPCs formed unorganized clusters with

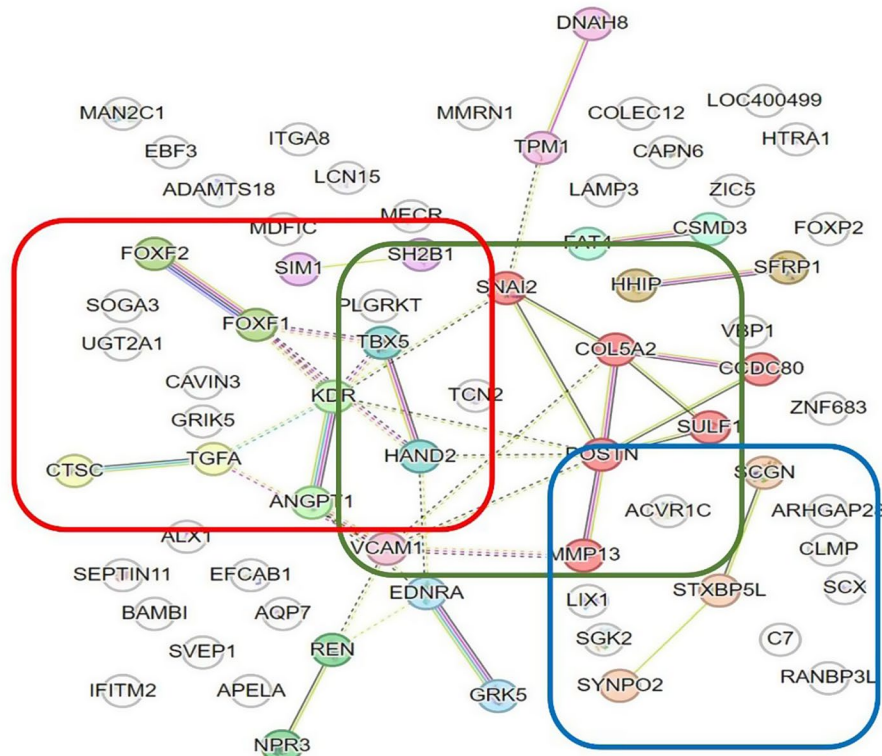
limited integration. Although all groups exhibited successful cell engraftment, blood C-peptide levels remained significantly lower than normal human levels, indicating the need for prolonged maturation (Fig. 7B).

To assess the biocompatibility of the esterified collagen hydrogel, we evaluated its degradation profile in vivo. Subcutaneous implantation in rats showed a rapid degradation rate, with over 50% of the hydrogel degrading within one week and complete absorption by 70 days (Fig. 7C).

Discussion

Our study focused on the crucial role of 3D culture and the ECM environment in the differentiation and maturation of IPCs derived from iPSCs due to their ability to mimic the physiological environment of pancreatic tissues more accurately [24]. In pancreatic tissue engineering, various polymers and matrix proteins, including collagen [18, 19, 25], laminin [26], alginate [11], and polyethylene glycol (PEG) [27], play crucial roles beyond structural support, influencing cell functionality. While previous research has explored ECM components, limited knowledge is available about the specific matrix that optimally supports IPC cell differentiation. Cultivating immature precursor cells, such as differentiated cells from stem cells, especially in comparison with adult

(A)



(B)

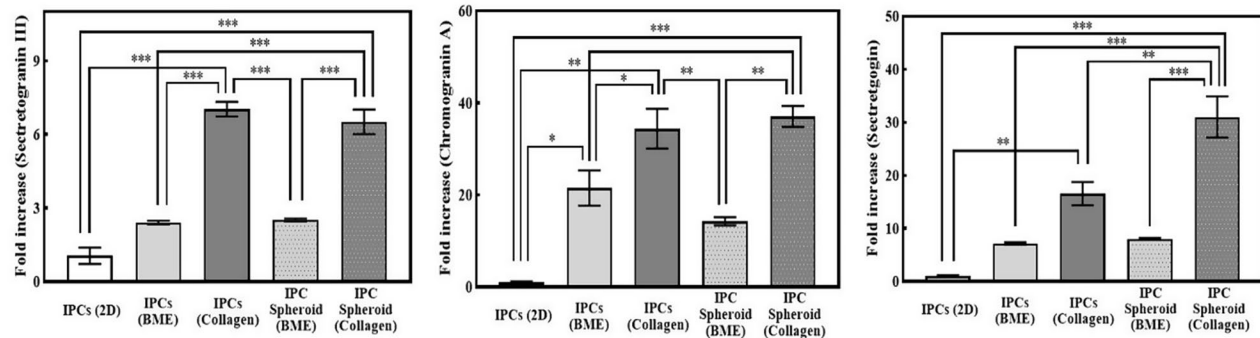


Fig. 6 Gene Expression Analysis and Pathway Involvement in IPC Spheroids Cultured in Collagen and BME Hydrogels **(A)** Network visualization of gene interactions based on microarray analysis, highlighting the differential gene expression in IPC spheroids embedded in collagen compared to BME hydrogels. Key genes with more than two-fold expression changes are emphasized. The gene network is represented by color-coded squares, where a red square denotes genes related to pancreas development and growth factors, a green square signifies genes associated with cell-cell and cell-ECM interactions, and a blue square highlights genes involved in granule formation and secretion. **(B)** Relative mRNA expression analysis of secretogranin III, chromogranin A, and secretogranin validates the microarray findings, confirming their elevated expression in collagen hydrogel cultures, particularly in IPC spheroids. The expression levels are shown to be significantly increased compared to those in BME and 2D cultures, underscoring their role in the maturation and functional enhancement of IPC spheroids cultured in collagen hydrogels. Statistical significance is indicated by asterisks (* $p < 0.05$, $n = 3$)

islets, necessitates a detailed analysis and application of the culture environment's physical and chemical properties to prevent undesirable differentiation pathways or compromise the functionality of the differentiated cells.

Currently, basement membrane matrixes, known commercially as BME and Matrigel, are commonly used for

3D cultures. However, they present challenges for clinical applications and may not accurately mimic the natural composition of the pancreas. This limitation is primarily attributed to their derivation from mouse tumor tissues. Proteomic profiling of human pancreatic tissues across different developmental stages revealed an enriched

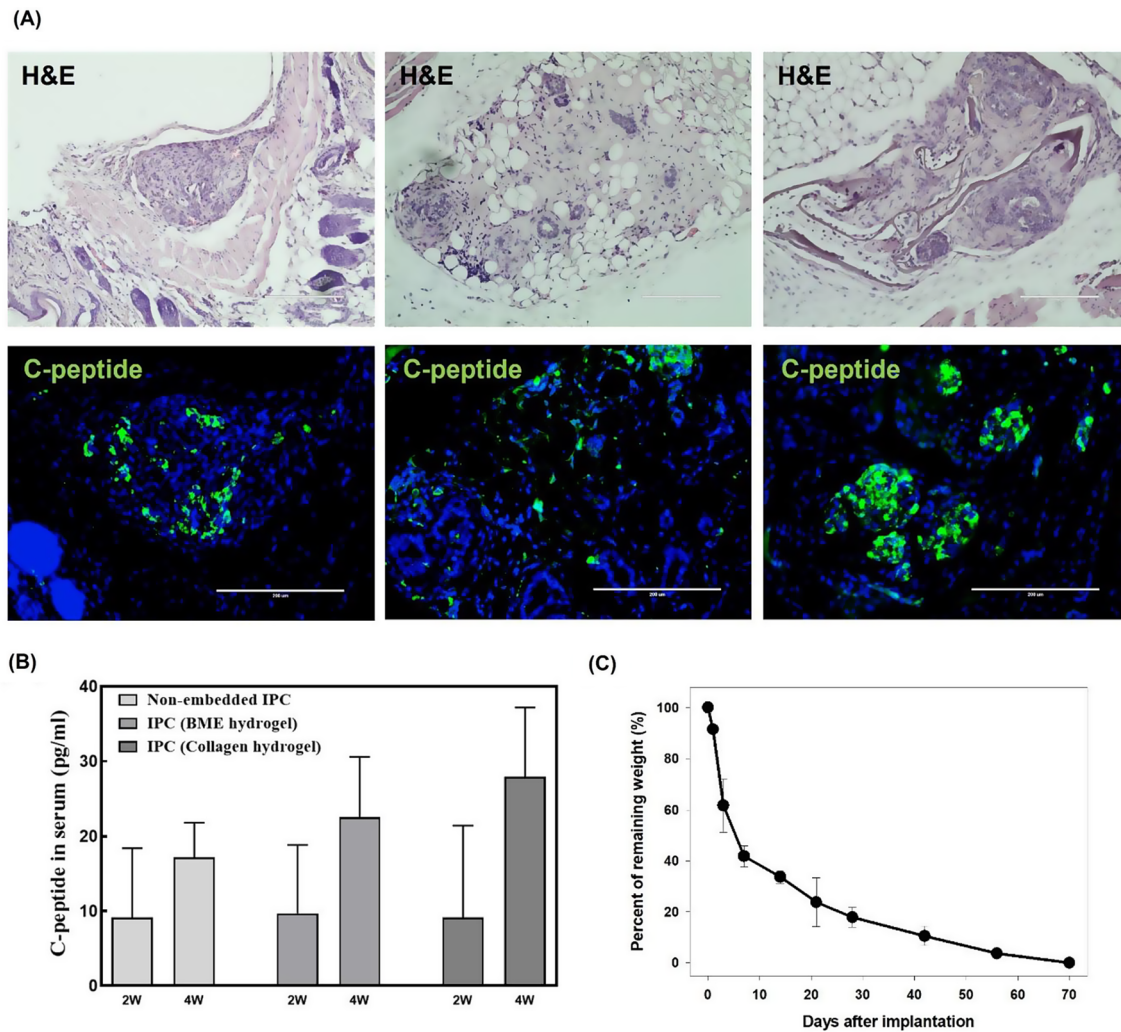


Fig. 7 In Vivo Assessment of IPC Spheroids and Esterified Collagen Hydrogel (A) Histological analysis (H&E and C-peptide staining) of subcutaneously implanted IPC spheroids in diabetic nude mice. The BME group exhibited duct-like structure formation, while the collagen group maintained spheroid integrity and demonstrated improved tissue integration. Scale bars: 200 μ m. Magnification: 20x. (B) Blood C-peptide levels in diabetic nude mice at 2- and 4-weeks post-implantation. (C) In vivo degradation rate of esterified collagen hydrogel. Over 50% of the hydrogel degraded within 7 days, with complete absorption by day 70

presence of ECM proteins such as COL12A1, COL14A1, and COL5A1, particularly in fetal and juvenile tissues, suggesting their integral involvement in organ maturation [28]. Additionally, ECM proteins like COL2A1, LAMA4, EMILIN1, and FN1 exhibited high expression levels in fetal and juvenile stages, with a decline noted in adult tissues. While decellularized pancreatic matrixes have shown promise in enhancing islet function, their mass production remains challenging [29–31]. Considering the potential for clinical application, ease of use, and the ECM protein compositions of the pancreas, collagen hydrogels can be considered a promising candidate material. Previous research, including our own, has highlighted the potential of collagen, especially ionized neutral collagen, in supporting the function and transplantation of islet cells and IPCs [18, 19]. Compared to

BME or Matrigel, which are derived from mouse tumor tissues and commonly used in existing research, collagen is already widely used in clinical settings, ensuring its safety. Additionally, its superior physical properties make it suitable for use as a scaffold or carrier in cell therapy applications.

In clinical settings, collagen hydrogels are often used at a viscosity of 3% or higher to increase retention, commonly in surgical and orthopedic operations. Our study optimized the concentration suitable for in vitro 3D culture. We found that 1–1.5% collagen concentrations are optimal for in vitro 3D cultures, allowing effective gelation at 37°C without compromising cell viability. Lower viscosities failed to gel, and higher concentrations led to excessive viscosity that could cause cell death. Our selection of a 1.5% collagen concentration was based on

its ability to form a porous network, essential for stable, long-term culture. This concentration was optimal for maintaining structural integrity and facilitating cell-laden capacity, as confirmed through rheological analysis and SEM observations. Not only the physical properties of the materials but also their chemical composition can significantly affect the cells. In this study, protein analysis was conducted to determine the protein composition of the collagen hydrogel and BME.

We assessed the effectiveness of collagen hydrogel as a scaffold for differentiating and maturing IPCs derived from iPSCs, in comparison to BME hydrogel. The observed differences in morphological characteristics and cellular distribution between IPCs and IPC spheroids in collagen versus BME hydrogels can be attributed to their unique physical properties and protein compositions. IPCs and IPC spheroids cultured in BME exhibited an increased formation of cyst-like structures over extended culture periods, particularly evident in spheroid cultures. This phenomenon could be attributed to the composition of BME, which primarily consists of laminin $\alpha 1$, $\beta 1$, and $\gamma 1$. These laminin structures predominantly appear around blood vessels and ductal structures during pancreatic development, representing a type of laminin different from that found in islet cells, potentially promoting the formation of duct-like structures [32]. Further research is required to explore this hypothesis. Additionally, BME's susceptibility to degradation by matrix metalloproteinases (MMPs) secreted from cells might contribute to the dissolution of the surrounding hydrogel, revealing cyst formation. Collagen hydrogels, however, supported the intact spheroidal shape of IPCs without cyst formation, due to their resistance to MMP degradation and their specific composition. Moreover, IPC spheroids in collagen demonstrated better insulin expression and cell–cell interactions, forming densely packed clusters of insulin-expressing cells, unlike the isolated cells and sporadic insulin expression observed in BME cultures.

Our study also demonstrated the ability of collagen hydrogel to significantly enhance the expression of genes related to IPC differentiation. The expression of PDX1, a key pancreatic differentiation factor [33], was increased in the hydrogel groups compared to that in 2D cultures, with a notable rise observed in collagen. Early stages (Day 5) showed no significant difference in endocrine-related gene expression in single cells; however, a marked increase was evident by day 10 in hydrogels. Spheroid encapsulation in hydrogels led to rapid endocrine expression from day 5, underscoring the importance of 3D spheroid structures in enhancing endocrine differentiation. Unlike that during the differentiation toward undesired cell types, the expression of ductal markers like CK19 remained unaffected, while glucagon levels rose,

suggesting broad endocrine cell differentiation enhancement. This underscores the need for targeted differentiation protocols toward IPCs. Key transcription factors pivotal for progression from progenitor to late-stage IPCs, including NGN3 [34], NKX2.1, and NKX6.1 [35], showed increased expression in the collagen group. Notably, NKX6.1, expressed only in mature cells, showed a similar or slightly lower trend when IPCs were encapsulated as single cells compared to that in 2D culture but showed a more than five-fold increase in IPC spheroids in the collagen group. This upregulation indicates the synergy of cell–cell and cell–ECM interactions in 3D cultures. Insulin and c-peptide secretion analyses further validated these findings, positioning IPC spheroids closer to an islet-like state, especially in collagen hydrogels, which significantly enhanced functional outcomes. This pronounced insulin response to glucose in collagen-embedded cells underscores the critical role of a 3D matrix in simulating a natural islet setting. These insights reveal that collagen hydrogels offer a more effective and biomimetic strategy for IPC cultivation and advancement over BME hydrogels, facilitating better differentiation and maturation into functional endocrine cells.

To investigate the underlying mechanisms by which collagen hydrogels enhance glucose responsiveness and maturation markers compared to BME hydrogels, gene expression profiles of IPC spheroids derived from both hydrogel environments were subjected to microarray analysis. Examination of differentially expressed genes (DEGs) exceeding a two-fold change via STRING analysis provided insight into the pivotal mechanisms involved. A notable increase in the expression of genes related to granule formation, insulin secretion, and ECM interactions suggests a synergistic effect that promotes IPC maturation within the collagen hydrogel's 3D structure. Importantly, genes involved in the creation of granules and hormone secretion showed heightened expression, likely aiding in the increased insulin secretion observed in response to glucose levels. Validation centered on assessing mRNA levels of secretogranin III [36], chromogranin A [37], and secretogin [38], which were all significantly higher in the collagen environment. This upregulation within IPC spheroids cultured in collagen hydrogels reveals the genetic basis for their enhanced maturation and functionality.

The use of esterified collagen hydrogel offers significant advantages for local retention and engraftment of differentiated cells *in vivo*. Unlike tumor-derived BME, collagen is widely used in medical applications, ensuring its safety. Its ability to dissolve in neutral media without requiring additional cross-linking makes it suitable for direct implantation. Our preliminary transplant results showed a improvement in cell engraftment, structural integrity, and insulin/C-peptide secretion in

collagen-embedded IPCs compared to non-embedded and BME-embedded IPCs. While C-peptide levels in diabetic animals were lower than normal human levels, indicating the need for longer maturation periods, the observed C-peptide secretion suggests high potential for blood glucose regulation with extended observation.

Although collagen is generally considered biocompatible, further studies are warranted to assess its long-term safety and potential immunogenicity. Additionally, while the hydrogel scaffold enables localized delivery, strategies to induce vascularization in subcutaneous tissue are essential for clinical translation. Our study highlights the potential of collagen hydrogels as a promising scaffold for IPC delivery. Future research should focus on long-term *in vivo* studies to evaluate glucose control, optimization of differentiation protocols, and development of strategies to enhance vascularization.

In conclusion, our investigation demonstrates the potential of collagen hydrogels as a conducive scaffold for the differentiation and maturation of iPSC-derived IPCs, offering promising prospects for cell-based therapeutic strategies for diabetes. The utilization of a physiologically relevant 3D microenvironment, as provided by collagen hydrogels, fulfills the structural and functional requirements of developing IPCs and activates essential signaling pathways for their functional maturation. These findings have significant implications for regenerative medicine, emphasizing the critical role of ECM mimetics in advancing cell therapy and tissue engineering applications.

Abbreviations

DM	Diabetes Mellitus
iPSCs	Induced Pluripotent stem cells
ECM	Extracellular matrix
GSIS	Glucose-stimulated insulin secretion
BME	Basement membrane extract
IPC	Insulin-producing cell
OCT4	Octamer-binding transcription factor 4
PDX1	Pancreatic and duodenal homeobox 1
FOXA2	Forkhead box protein A2
ISL1	Insulin gene enhancer protein
NKX2.2	NK2 homeobox 2
NKX6.1	NK6 homeobox 1
PE	Pancreatic progenitor
SEM	Scanning electron microscopy
GCG	Glucagon
SST	Somatostatin
CK19	Cytokeratin 19
COL	Collagen
LAMA	Laminin A
EMILIN	Elastin microfibril interface-located protein
FN	Fibronectin

Supplementary Information

The online version contains supplementary material available at <https://doi.org/10.1186/s13287-024-03971-2>.

Supplementary Material 1

Supplementary Material 2

Acknowledgements

Not applicable.

Author contributions

JEM and YNL: performed the experiments and analyzed the data, wrote and revised the manuscript. SJ, HRJ and HMM: technical support, analyzed the data. YJ and JJ performed experiments, provided data. SCK and IKS directed the study, critically revised, and contributed to manuscript approval. All authors have read and agreed to the published version of the manuscript.

Funding

This work was supported by a National Research Foundation of Korea (NRF) grant funded by the Korean government Ministry of Science and ICT (MSIT) (No. 2021R111A2048392). This work was supported by the Alchemist Project (20012378, Development of Meta Soft Organ Module Manufacturing Technology without Immunity Rejection and Module Assembly Robot System), the Ministry of Trade, Industry & Energy (MOTIE, Republic of Korea). This study was supported by the Korean Fund for Regenerative Medicine funded by the Ministry of Science and ICT and the Ministry of Health and Welfare (RS-2022-00080258, Republic of Korea). This study was supported by a grant (2021IP0083-1) from the Asan Institute for Life Sciences, Asan Medical Center, Seoul, Korea.

Data availability

The data that support the findings of this study are available on request from the corresponding author.

Declarations

Ethical approval

Induced pluripotent stem cells (iPSCs) were provided by the Center for Stem Cell Research, Asan Medical Center, Seoul, Korea, with ethical clearance from the Institutional Review Board (IRB: 2017–0503) granted on April 28, 2017, for the project titled “Development of Insulin-Producing Cells Differentiated from Embryonic Stem Cells and Induced Pluripotent Stem Cells.”

Consent for publication

Not applicable.

Conflict of interest

All authors declare no potential conflict of interest. The authors declare that there are no other financial or non-financial competing interests. The authors of the article do not have any commercial association (e.g., consultancies, stock ownership, equity interests, patent-licensing arrangements) that might pose a conflict of interest in connection with the submitted article.

Author details

¹Asan Institute for Life Sciences, Asan Medical Center, Seoul, Republic of Korea

²Asan Medical Center, Asan Medical Institute of Convergence Science and Technology (AMIST), University of Ulsan College of Medicine, 88 Olympic-ro 43-gil, Songpa-gu, Seoul 05505, Republic of Korea

³School of Interdisciplinary Bioscience and Bioengineering (POSTECH), Pohang 37673, Republic of Korea

⁴Department of Mechanical Engineering (POSTECH), Pohang 37673, Republic of Korea

⁵Department of Biomedical Engineering, University of Ulsan College of Medicine, Seoul, Republic of Korea

⁶Division of Hepatobiliary and Pancreatic Surgery, Department of Surgery, Asan Medical Center, University of Ulsan College of Medicine, Brain Korea 21 Project, Seoul, Korea

Received: 25 March 2024 / Accepted: 1 October 2024

Published online: 23 October 2024

References

1. American Diabetes Association Professional Practice. 2. Classification and diagnosis of diabetes: standards of Medical Care in Diabetes-2022. *Diabetes Care*. 2022;45(Suppl 1):S17–38.
2. Ryan EA, et al. Beta-score: an assessment of beta-cell function after islet transplantation. *Diabetes Care*. 2005;28(2):343–7.
3. Shapiro AM, Pokrywczynska M, Ricordi C. Clinical pancreatic islet transplantation. *Nat Rev Endocrinol*. 2017;13(5):268–77.
4. Fiorina P, et al. The clinical impact of islet transplantation. *Am J Transpl*. 2008;8(10):1990–7.
5. Zalzman M, Anker-Kitai L, Efrat S. Differentiation of human liver-derived, insulin-producing cells toward the beta-cell phenotype. *Diabetes*. 2005;54(9):2568–75.
6. Zhang D, et al. Highly efficient differentiation of human ES cells and iPS cells into mature pancreatic insulin-producing cells. *Cell Res*. 2009;19(4):429–38.
7. Hering BJ, et al. Phase 3 Trial of Transplantation of Human Islets in type 1 diabetes complicated by severe hypoglycemia. *Diabetes Care*. 2016;39(7):1230–40.
8. Ryan EA, et al. Five-year follow-up after clinical islet transplantation. *Diabetes*. 2005;54(7):2060–9.
9. Lammert E, Thorn P. The role of the Islet Niche on Beta Cell structure and function. *J Mol Biol*. 2020;432(5):1407–18.
10. Cabrera O, et al. The unique cytoarchitecture of human pancreatic islets has implications for islet cell function. *Proc Natl Acad Sci U S A*. 2006;103(7):2334–9.
11. Llacua A, et al. Extracellular matrix components supporting human islet function in alginate-based immunoprotective microcapsules for treatment of diabetes. *J Biomed Mater Res A*. 2016;104(7):1788–96.
12. Jiang K, et al. 3-D physiometric extracellular matrix hydrogels provide a supportive microenvironment for rodent and human islet culture. *Biomaterials*. 2019;198:37–48.
13. Smink AM, de Vos P. Therapeutic strategies for modulating the Extracellular Matrix to improve pancreatic islet function and survival after transplantation. *Curr Diab Rep*. 2018;18(7):39.
14. Artym VV, Matsumoto K. *Imaging cells in three-dimensional collagen matrix*. *Curr Protoc Cell Biol*, 2010. Chapter 10: p. Unit 10 18 1–20.
15. Riopel M, Wang R. Collagen matrix support of pancreatic islet survival and function. *Front Biosci (Landmark Ed)*. 2014;19(1):77–90.
16. Cheng JY, et al. Matrix components and scaffolds for sustained islet function. *Tissue Eng Part B Rev*. 2011;17(4):235–47.
17. Davis NE, et al. Enhanced function of pancreatic islets co-encapsulated with ECM proteins and mesenchymal stromal cells in a silk hydrogel. *Biomaterials*. 2012;33(28):6691–7.
18. Ko JH, et al. Collagen esterification enhances the function and survival of pancreatic beta cells in 2D and 3D culture systems. *Biochem Biophys Res Commun*. 2015;463(4):1084–90.
19. Kim YH et al. Long-term reversal of diabetes by subcutaneous transplantation of pancreatic islet cells and adipose-derived stem cell sheet using surface-immobilized heparin and engineered collagen scaffold. *BMJ Open Diabetes Res Care*. 2020. 8(1).
20. Hintze V, Schnabelrauch M, Rother S. Chemical modification of Hyaluronan and their Biomedical Applications. *Front Chem*. 2022;10:830671.
21. Temiz A, et al. Esterified hyaluronic acid improves cartilage viability in experimental tracheal reconstruction with an auricular graft. *Otolaryngol Head Neck Surg*. 2010;143(6):772–8.
22. Kunisada Y, et al. Small molecules induce efficient differentiation into insulin-producing cells from human induced pluripotent stem cells. *Stem Cell Res*. 2012;8(2):274–84.
23. Hogrebe NJ, et al. Generation of insulin-producing pancreatic β cells from multiple human stem cell lines. *Nat Protoc*. 2021;16(9):4109–43.
24. Ikemoto T, et al. In vitro and in vivo effects of insulin-producing cells generated by xeno-antigen free 3D culture with RCP piece. *Sci Rep*. 2019;9(1):10759.
25. Zhu Y, et al. Collagen type I enhances cell growth and insulin biosynthesis in rat pancreatic cells. *J Mol Endocrinol*. 2021;67(3):135–48.
26. Sigmundsson K, et al. Culturing functional pancreatic islets on alpha5-laminins and curative transplantation to diabetic mice. *Matrix Biol*. 2018;70:5–19.
27. Ghasemi A, Akbari E, Imani R. An overview of Engineered Hydrogel-based biomaterials for improved beta-cell survival and insulin secretion. *Front Bioeng Biotechnol*. 2021;9:662084.
28. Li Z, et al. Proteome-wide and matrisome-specific alterations during human pancreas development and maturation. *Nat Commun*. 2021;12(1):1020.
29. Salg GA, et al. The emerging field of pancreatic tissue engineering: a systematic review and evidence map of scaffold materials and scaffolding techniques for insulin-secreting cells. *J Tissue Eng*. 2019;10:2041731419884708.
30. Guruswamy Damodaran R, Vermette P. Decellularized pancreas as a native extracellular matrix scaffold for pancreatic islet seeding and culture. *J Tissue Eng Regen Med*. 2018;12(5):1230–7.
31. Kim J et al. Pancreatic tissue-derived Extracellular Matrix Bioink for Printing 3D cell-Laden pancreatic tissue constructs. *J Vis Exp*, 2019;154.
32. Heymans C, et al. Pancreatic acinar differentiation is guided by differential laminin deposition. *Sci Rep*. 2019;9(1):2711.
33. Zhu Y et al. *PDX1, Neurogenin-3, and MAFA: critical transcription regulators for beta cell development and regeneration*. *Stem Cell Res Ther*, 2017. 8(1): p. 240.
34. Churchill AJ et al. Genetic evidence that Nkx2.2 acts primarily downstream of Neurog3 in pancreatic endocrine lineage development. *Elife*. 2017;10(6):e20010.
35. Aigha II, Abdelalim EM. NKX6.1 transcription factor: a crucial regulator of pancreatic beta cell development, identity, and proliferation. *Stem Cell Res Ther*. 2020;11(1):459.
36. Lin CC et al. Serum secretogranin III concentrations were increased in subjects with metabolic syndrome and independently Associated with Fasting plasma glucose levels. *J Clin Med*, 2019. 8(9).
37. Wollam J, et al. Chromogranin A regulates vesicle storage and mitochondrial dynamics to influence insulin secretion. *Cell Tissue Res*. 2017;368(3):487–501.
38. Sharma AK, et al. Secretagogen regulates insulin signaling by direct insulin binding. *iScience*. 2019;21:736–53.

Publisher's note

Springer Nature remains neutral with regard to jurisdictional claims in published maps and institutional affiliations.